



Spectral studies and crystal structures of molybdenum(VI) complexes containing pyridine or picoline as auxiliary ligands: interaction energy calculations and free radical scavenging studies

Daly Kuriakose¹ · M. R. Prathapachandra Kurup^{1,2}

Received: 17 September 2020 / Accepted: 4 November 2020
© Springer Nature Switzerland AG 2020

Abstract

Three *cis*-MoO₂ complexes [MoO₂(CAB)(py)] (**1**), [MoO₂(CAB)(3-pic)] (**2**) and [MoO₂(CAB)(4-pic)] (**3**) which vary in the nature of the heterocyclic bases in the auxiliary coordination site derived from an ONO donor aroylhydrazone (H₂CAB) have been synthesized and characterized by various physicochemical methods. The single-crystal X-ray diffraction studies reveal that the complexes adopt a distorted octahedral N₂O₄ coordination sphere around the Mo(VI) center in which the ONO donor atoms of hydrazone moiety and one oxido oxygen constitute the NO₃ basal plane and the axial position by the other oxido oxygen and nitrogen atom of coordinated pyridine molecule in [MoO₂(CAB)(py)] (**1**) or picoline molecule in [MoO₂(CAB)(3-pic)] (**2**) and [MoO₂(CAB)(4-pic)] (**3**). The hydrogen bonding interaction generates a two-dimensional supramolecular sheet-like architecture in [MoO₂(CAB)(py)] (**1**) and [MoO₂(CAB)(3-pic)] (**2**), whereas a three-dimensional network was observed in [MoO₂(CAB)(4-pic)] (**3**). The interaction energy calculations reveal that the dispersion energy component dominates over other components and [MoO₂(CAB)(3-pic)] (**2**) is found to be energetically more stable. Furthermore, the aroylhydrazone shows free radical scavenging activity, whereas the complexes are inactive.

Introduction

Aroylhydrazones are well-established class of molecules with several possible structures including configurational isomers, viz. *E* and *Z*, around the imine (C=N) bond and amido/iminol tautomers. Due to the presence of multiple donor sites such as protonated/deprotonated amide oxygen, imine nitrogen and additional donor site (usually N or O) provided from the carbonyl compound, they exhibit diverse chelating modes with greater effects in a wide variety of fields [1–4]. The presence of the azomethine group (–NH–N=CH–) connected with carbonyl group makes them

responsible for different biological activities, such as anti-oxidant, anti-inflammatory, anti-hypertensive, antimicrobial and anticancer properties [5–10]. Among transition metals, the chemistry of molybdenum has become an important area due to its potential application in diverse fields [11–15]. Molybdenum complexes have a unique place in the advancement of coordination chemistry [16]. Due to their extended applicability in biology and pharmacology, complexes containing pyridine ring moieties are of great interest [17–20]. The field of supramolecular architecture is very important in coordination chemistry. Various supramolecular interactions including conventional and non-conventional hydrogen bonds and non-covalent interactions such as π – π interactions, C–H \cdots π , anion (halide) \cdots π and even C–H \cdots C interactions gave rise to a number of 1D, 2D and 3D supramolecular architectures [21–23].

Due to their facile synthesis, structural flexibility, stability and high potential as efficient catalysts, a great deal of work has been carried out on the synthesis and characterization of *cis*-dioxidomolybdenum(VI) complexes containing the [MoO₂]²⁺ core [24–26]. The articles regarding the biological activities of molybdenum complexes are, however, much more limited. The present study reports the syntheses, spectral and structural characterization of *cis*-MoO₂

Electronic supplementary material The online version of this article (<https://doi.org/10.1007/s11243-020-00440-6>) contains supplementary material, which is available to authorized users.

✉ M. R. Prathapachandra Kurup
mrpcusat@gmail.com; mrp@cukerala.ac.in

¹ Department of Applied Chemistry, Cochin University of Science and Technology, Kochi, Kerala 682 022, India

² Department of Chemistry, School of Physical Sciences, Central University of Kerala, Tejaswini Hills, Periyar, Kasaragod, Kerala 671 320, India

complexes of an ONO-donor aroylhydrazone ligand, which differ in the presence of neutral N-donor heterocyclic bases in the auxiliary coordination site. We also report free radical scavenging studies of the ligands and complexes, herein.

Experimental procedure

Materials

The chemicals and solvents used in the syntheses were used without further purification. The chemicals, 3',5'-dichloro-2'-hydroxyacetophenone (Aldrich), 3-methoxybenzhydrazide (Alfa Aesar) and bis(acetylacetonato)dioxomolybdenum(VI) (Aldrich) used were of analar quality. Methanol, pyridine, 3-picoline and 4-picoline were purchased from Spectrochem. The aroylhydrazone ($H_2CAB \cdot H_2O$) was synthesized by a previously reported procedure [27].

Synthesis details

Synthesis of 3',5'-dichloro-2'-hydroxyacetophenone-3-methoxybenzoylhydrazone monohydrate ($H_2CAB \cdot H_2O$)

3-Methoxybenzhydrazide (0.17 g, 1.00 mmol) dissolved in 10 mL methanol, 3',5'-dichloro-2'-hydroxyacetophenone (0.21 g, 1.00 mmol) dissolved in 10 mL methanol was added and refluxed for 4 h. Single crystals suitable for X-ray analysis obtained on evaporation of the resulting reaction mixture were separated, washed and dried over P_4O_{10} in vacuo [27].

Analytical data for $C_{16}H_{16}Cl_2N_2O_4$ ($H_2CAB \cdot H_2O$) Yield: 0.29 g (77%); color: Yellow; M.W.: 371.21 g mol⁻¹; elemental analysis calculated/found (%): C 51.8/51.7, H 4.3/4.5, N 7.6/7.8; ¹H NMR (400 MHz, DMSO-*d*₆): δ 2.86 (3H, *s*, -CH₃), 3.85 (3H, *s*, -OCH₃), 7.22 (1H, *q*, aromatic), 7.5 (3H, *m*, aromatic), 7.63 (1H, *d*, aromatic), 7.68 (1H, *d*, aromatic), 11.55 (1H, *br*, OH), 14.43 (1H, *br*, NH); FT-IR: ν (cm⁻¹) 3548 ν(O-H), 3439 ν(N-H), 1660 ν(C=O), 1592, ν(C=N).

Synthesis of molybdenum(VI) complexes

Synthesis of [MoO₂(CAB)(py)] (1), [MoO₂(CAB)(3-pic)] (2) and [MoO₂(CAB)(4-pic)] (3)

For 10 mL methanolic solution of 3-methoxybenzhydrazide (0.17 g, 1.00 mmol), 10 mL methanolic solution of 3',5'-dichloro-2'-hydroxyacetophenone (0.21 g, 1.00 mmol) is added and refluxed for 3 h. Bis(acetylacetonato)dioxomolybdenum(VI) (0.33 g, 1.00 mmol) dissolved in 10 mL methanol was added slowly to the above refluxing solution, and refluxation was continued for another 30 min. For the refluxing solution, 0.5 mL of respective heterocyclic base (pyridine for complex 2 and 3-picoline for complex 3

and 4-picoline for complex 4) was added and refluxed again for 2½ h. Single crystals suitable for X-ray analysis obtained on slow evaporation of the resulting orange colored solutions were filtered off and washed with methanol and dried over P_4O_{10} in vacuo (Scheme 1).

Analytical data for $C_{21}H_{17}Cl_2MoN_3O_5$ ([MoO₂(CAB)(py)] (1): Yield: 0.34 g (61%); color: orange; M.W.: 558.22 g mol⁻¹; elemental analysis calculated/found (%): C 45.2/45.3, H 3.1/3.1, N 7.5/7.5; ¹H NMR (400 MHz, DMSO-*d*₆): δ 2.96 (3H, *s*, -CH₃), 3.89 (3H, *s*, -OCH₃), 7.23–8.64 (11H, aromatic); FT-IR: ν (cm⁻¹) 1583 and 1545 ν(C=N), 1337 ν(C-O), 935 and 921 ν(Mo=O).

Analytical data for $C_{22}H_{19}Cl_2MoN_3O_5$ ([MoO₂(CAB)(3-pic)] (2): Yield: 0.39 g (68%); color: orange; M.W.: 572.24 g mol⁻¹; elemental analysis calculated/found (%): C 46.2/46.1, H 3.4/3.3, N 7.3/7.3; ¹H NMR (400 MHz, DMSO-*d*₆): δ 2.35 (3H, *s*, -CH₃ (3-pic)), 2.96 (3H, *s*, -CH₃), 3.89 (3H, *s*, -OCH₃), 7.22–8.47 (10H, aromatic); FT-IR: ν (cm⁻¹) 1590 and 1547 ν(C=N), 1335 ν(C-O), 925 and 853 ν(Mo=O).

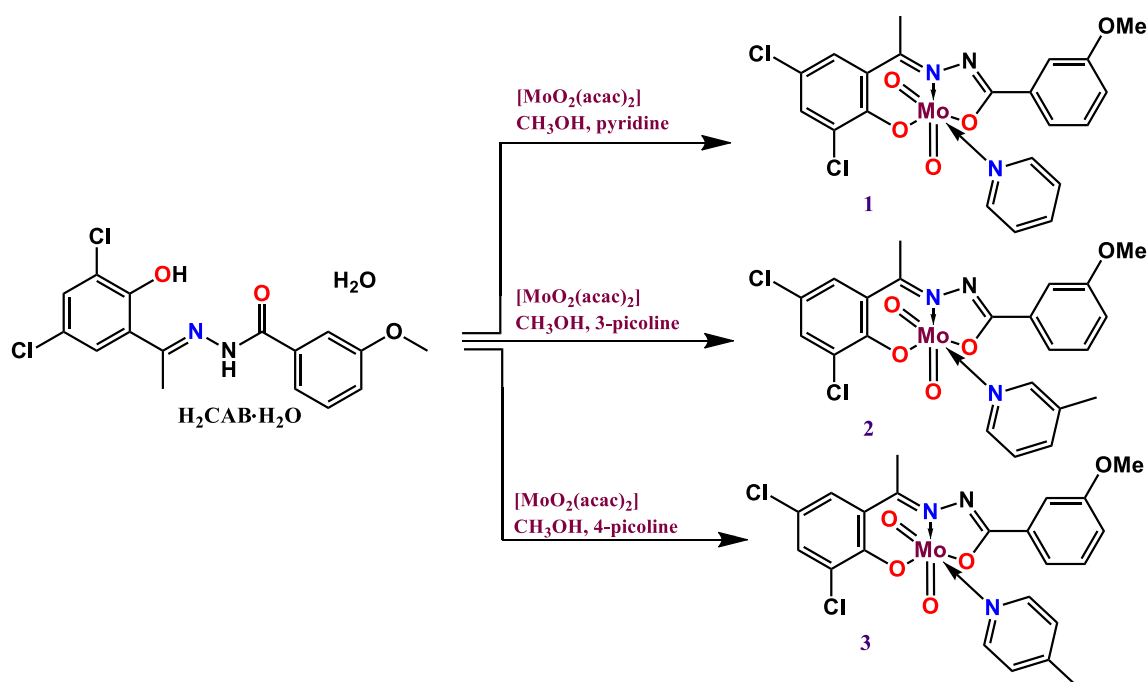
Analytical data for $C_{22}H_{19}Cl_2MoN_3O_5$ ([MoO₂(CAB)(4-pic)] (3): Yield: 0.34 g (59%); color: orange; M.W.: 572.24 g mol⁻¹; elemental analysis calculated/found (%): C 46.2/46.3, H 3.4/3.5, N 7.3/7.4; ¹H NMR (400 MHz, DMSO-*d*₆): δ 2.32 (3H, *s*, -CH₃ (4-pic)), 2.91 (3H, *s*, -CH₃), 3.84 (3H, *s*, -OCH₃), 7.18–8.43 (10H, aromatic); FT-IR: ν (cm⁻¹) 1591 and 1545 ν(C=N), 1333 ν(C-O), 927 and 914 ν(Mo=O).

Physical measurements

The micro-analyses of carbon, hydrogen and nitrogen were performed on a Vario EL III CHNS analyzer. IR spectra of the compounds were recorded in KBr pellets with FTIR spectrometer (JASCO-4100) in the region 4000–400 cm⁻¹. The proton NMR spectra were collected in DMSO-*d*₆ on a Bruker Avance III, 400 MHz spectrometer having 9.4 T superconducting magnet using tetramethylsilane (TMS) as an internal reference. Electronic spectra in DMF solutions were recorded on a Thermo scientific evolution 201 UV-Vis double beam spectrophotometer in the 200–800 nm range.

Crystallographic data collection and refinement

Single crystals of the Mo(VI) complexes, [MoO₂(CAB)(py)] (1), [MoO₂(B)(3-pic)] (2) and [MoO₂(CAB)(4-pic)] (3) with suitable dimensions were mounted on a Bruker SMART APEXII charge-coupled device (CCD) diffractometer, equipped with a graphite crystal, incident-beam monochromator with Mo Kα (λ=0.71073 Å) radiation as the X-ray source. The data collection was performed at 293 K. Data reduction was performed using the program Bruker SAINT. APEX2 and SAINT were used for cell refinement



Scheme 1 Synthetic route for complexes **1–3**

[28]. Absorption corrections were carried out using SADABS based on Laue symmetry using equivalent reflections [29]. The structure was solved by using SHELXS-97 direct methods and refined by full-matrix least-squares refinement on F^2 using SHELXL-2018/1 [30] as well as WinGX software package [31]. The molecular and crystal structures were plotted using ORTEP-3 [31], DIAMOND version 3.2 g [32] and MERCURY 3.10.1 software [33]. Non-hydrogen atoms were refined anisotropically. All H atoms on C were repositioned in their calculated positions, guided by difference maps, with C–H bond distances 0.93–0.96 Å. H atoms were assigned as $U_{\text{iso}} = 1.2U_{\text{eq}}$ (1.5 for Me). Some reflections were omitted owing to bad agreement. The crystallographic data and structure refinement parameters for complexes **1**, **2** and **3** are given in Table 1.

Hirshfeld surface analysis

The Hirshfeld surface (HS) analysis and the associated 2D fingerprint plot were performed using the program Crystal-Explorer 17.5 by inputting CIF (crystallographic information file) [34]. The normalized contact distance (d_{norm}) was mapped over a color scale of -0.348 Å (red) to $+2$ Å (blue) for complexes. The shape index was mapped in the fixed color range -1 to 1 Å and curvedness in the range -4 to 4 Å. The normalized contact distance (d_{norm}) was based on d_e and d_i and van der Waals radii of the atoms. It is given by

$$d_{\text{norm}} = \frac{d_i - r_i^{\text{vdW}}}{r_i^{\text{vdW}}} + \frac{d_e - r_e^{\text{vdW}}}{r_e^{\text{vdW}}}$$

where d_e is the distance from any surface point to the nearest nucleus external to the surface, and d_i is defined as the distance to the nearest nucleus internal to the surface, respectively. r_i^{vdW} and r_e^{vdW} are the van der Waals radii of the atoms. The d_{norm} surfaces are displayed as red–white–blue (shorter than vdW–equal to vdW–longer than vdW separation, respectively) color code. The particular atom pair contacts are highlighted by deconstructing the pseudo-mirrored 2D fingerprint plots [35–37]. The d_i vs d_e fingerprint plots were displayed in the range 0.6–2.8 Å including reciprocal contact.

Interaction energy calculations and energy framework analysis

The interaction energies were calculated for a cluster of radius 3.8 Å generated around the molecule present in the asymmetric unit. The interaction energy calculations (E_{tot}) between the molecules are obtained using monomer wavefunctions calculated at the HF/3-21G level using symmetry-independent molecule with scale factors to determine E_{tot} : $k_{\text{ele}} = 1.019$, $k_{\text{pol}} = 0.651$, $k_{\text{dis}} = 0.901$ and $k_{\text{rep}} = 0.811$ [38]. The energies are expressed in terms of electrostatic (E'_{ele}),

Table 1 Crystallographic data and structure refinement for Mo(VI) complexes **1**, **2** and **3**

Parameters	1	2	3
Empirical formula	C ₂₁ H ₁₇ Cl ₂ MoN ₃ O ₅	C ₂₂ H ₁₉ Cl ₂ MoN ₃ O ₅	C ₂₂ H ₁₉ Cl ₂ MoN ₃ O ₅
Formula weight	558.22	572.24	572.24
Crystal system, space group	Monoclinic, <i>P</i> 2 ₁ / <i>c</i>	Monoclinic, <i>P</i> 2 ₁ / <i>n</i>	Orthorhombic, <i>Pbca</i>
<i>Cell parameters</i>			
<i>a</i> (Å)	12.8549 (8)	7.8667 (10)	14.1119 (7)
<i>b</i> (Å)	11.7903 (7)	14.344 (2)	16.6927 (9)
<i>c</i> (Å)	16.1183 (9)	20.433 (3)	19.4198 (10)
α (°)	90°	90°	90°
β (°)	112.774 (3)°	97.097 (5)°	90°
γ (°)	90°	90°	90°
Volume <i>V</i> (Å ³)	2252.5 (2)	2287.9 (5)	4574.6 (4)
<i>Z</i>	4	4	8
Calculated density (ρ) (Mg m ⁻³)	1.646	1.661	1.662
Absorption coefficient, μ (mm ⁻¹)	0.858	0.847	0.847
<i>F</i> (000)	1120	1152	2304
Crystal size (mm)	0.3 × 0.25 × 0.2	0.4 × 0.35 × 0.2	0.35 × 0.25 × 0.2
Reflections collected/unique reflections (<i>R</i> _{int})	26,661/5697 [<i>R</i> (int)=0.0323]	27,964/5710 [<i>R</i> (int)=0.0339]	52,714/5712 [<i>R</i> (int)=0.0401]
Completeness to θ	25.242 (99.9%)	25.242 (99.9%)	25.242 (99.9%)
Maximum and minimum transmission	0.842 and 0.814	0.776 and 0.72	0.844 and 0.816
Data/restraints/parameters	5697/0/289	5710/0/298	5712/0/301
Goodness of fit on <i>F</i> ²	1.038	1.066	1.121
Final <i>R</i> indices [<i>I</i> > 2 σ (<i>I</i>)]	<i>R</i> ₁ = 0.0326, <i>wR</i> ₂ = 0.0768	<i>R</i> ₁ = 0.0325, <i>wR</i> ₂ = 0.0850	<i>R</i> ₁ = 0.0478, <i>wR</i> ₂ = 0.1173
<i>R</i> indices (all data)	<i>R</i> ₁ = 0.0531, <i>wR</i> ₂ = 0.0871	<i>R</i> ₁ = 0.0426, <i>wR</i> ₂ = 0.0899	<i>R</i> ₁ = 0.0690, <i>wR</i> ₂ = 0.1342
Largest difference peak and hole (e Å ⁻³)	0.680 and -0.495	0.518 and -0.527	0.615 and -0.631
$R1 = \sum F_o - F_c / \sum F_o $		$wR_2 = [\sum w(F_o^2 - F_c^2)^2 / \sum w(F_o^2)^2]^{1/2}$	

polarization (E'_{pol}), dispersion (E'_{dis}) and exchange repulsion (E'_{rep}) terms [39]. The total energy (E_{tot}) is represented as

$$E_{\text{tot}} = k_{\text{ele}}E'_{\text{ele}} + k_{\text{pol}}E'_{\text{pol}} + k_{\text{dis}}E'_{\text{dis}} + k_{\text{rep}}E'_{\text{rep}},$$

where the *k* values are scale factors.

The energy frameworks are the graphical representations of the magnitudes of the intermolecular interaction energies. The molecular pair-wise interaction energies are represented as cylinders joining the centroids of pairs of molecules. Frameworks were constructed for E_{elec} as red cylinders, E_{dis} as green and E_{tot} as blue.

Free radical scavenging studies

The free radical scavenging studies of the aroylhydrazone and the complexes were examined by DPPH ((2,2-diphenyl-1-picrylhydrazyl) assay. Different concentrations (10, 20, 30, 40 and 50 $\mu\text{g/mL}$) of the test compounds (dissolved in DMSO) and a methanolic blank were incubated at 37 °C with 187 μL of

freshly prepared DPPH (3 mg/25 mL methanol) for 30 min in dark. The absorbance was measured at 517 nm using UV–Vis spectrophotometer. The assay was carried out in triplicate, and the mean was reported. The concentration required to result in 50% inhibition (IC₅₀ value) was also calculated. The DPPH radical scavenging activity was calculated using the formula:

$$\% \text{ inhibition} = \frac{(A_0 - A_1)}{A_0} \times 100.$$

A_0 and A_1 = Absorbance at 517 nm of the radical (DPPH) in the absence and presence of antioxidant.

Results and discussion

The *cis*-MoO₂ complexes having the general formula [MoO₂(CAB)D] (D = pyridine (complex **1**), 3-picoline (complex **2**) and 4-picoline (complex **3**) were synthesized by refluxing solutions of [MoO₂(*acac*)₂] with aroylhydrazone in

the presence suitable heterocyclic bases. The complexes are stable toward air and moisture in the solid state at room temperature. The complexes are characterized using elemental analyses, IR, UV–Vis and ^1H NMR spectra. The molecular structures of complexes **1–3** are determined using SCXRD studies.

Spectral studies

The spectrum of aroylhydrazone was compared with the spectra of Mo(VI) complexes **1–3**, and the characteristic IR bands are displayed in Table S1. The two medium intensity broadbands at around 3548 and 3439 cm^{-1} allocated to stretching vibrations of O–H, N–H and a strong band at 1660 cm^{-1} due to $\nu(\text{C}=\text{O})$ mode in the ligand disappear upon complexation which indicate the coordination of phenolate and iminolate oxygen to the $[\text{MoO}_2]^{2+}$ core [40, 41]. Strong band assignable to $\nu(\text{C}=\text{N})$ observed at around 1592 cm^{-1} of the free aroylhydrazone was red shifted to 1583, 1590 and 1591 cm^{-1} , respectively, in the corresponding complexes indicating the coordination of azomethine nitrogen to the metal ion [40, 41]. Besides, the appearance of a new band assignable to asymmetric stretching vibration of newly formed C=N in the complexes in the range 1525–1550 cm^{-1} substantiates the existence of iminolate form of ligand in the complexes. The two absorption bands corresponding to symmetric and asymmetric stretching vibrations of $\nu(\text{Mo}=\text{O})$ of *cis*- MoO_2 were observed in the region 850–936 cm^{-1} [40, 41]. The pyridine stretching vibrations were observed in the range 1400–1500 cm^{-1} in complexes **1–3**.

The ^1H NMR spectra of dioxidomolybdenum(VI) complexes were recorded in DMSO- d_6 (Figs. S1–S4). After complexation, the resonance corresponding to protons attached to the nitrogen (N2) and oxygen (O1) disappeared indicating that the aroylhydrazone coordinates through phenolate and iminolate oxygens, O1 and O2. The aromatic protons show signals in the 7.2–8.3 ppm range. The resonance peaks assignable to $-\text{CH}_3$ group of picoline in complexes **2** and **3** were observed at 2.35 and 2.32 ppm, respectively.

The electronic spectra of molybdenum(VI) complexes were recorded in 1×10^{-5} M DMF solution, and the spectral assignments are summarized in Table S2 (Fig. S5). The electronic spectra of the complexes display absorption band probably due to $n \rightarrow \pi^*$ and $\pi \rightarrow \pi^*$ transitions involving molecular orbitals located on aromatic ring, azomethine nitrogen, etc., in the range 270–330 nm [42–44]. The $\text{O}(p\pi) \rightarrow \text{Mo}(d\pi)$ LMCT ligand-to-metal charge transfer transitions involving the promotion of an electron from the filled HOMO of the ligand to the empty LUMO of Mo were observed at 399, 396 and 415 nm, respectively, for complexes **1**, **2** and **3** [40, 41]. The absence of $d-d$ transition

bands in the visible region confirms the $4d^0$ electronic configuration of Mo(VI) moiety [40, 41].

Crystal structure analysis

Molecular structure descriptions of complexes **1–3**

The asymmetric unit of monomeric complexes **1–3** consists of only one molecule. In all the complexes, the molybdenum center is octahedrally coordinated by phenolate oxygen (O1), azomethine nitrogen (N1), iminolate oxygen (O2), two terminal oxido oxygen atoms (O4 and O5) and nitrogen atom (N3) of the monodentate N-donor auxiliary ligand (pyridine in complex **1**, 3-picoline in complex **2** or 4-picoline in complex **3**). The aroylhydrazone behaves as a dianionic tridentate ligand and coordinates to the molybdenum center in the iminolate form. Molecular structures and atom numbering scheme of complexes **1–3** are shown in Figs. 1, 2 and 3. Selected bond angles ($^\circ$) and bond distances (\AA) are listed on Table S1. Complexes **1** and **2** crystallized in monoclinic space groups $P2_1/c$ and $P2_1/n$, respectively, whereas complex **3** crystallized in orthorhombic space group $Pbca$. A comparison of the molecular structures of the metal free ligand and molybdenum complexes reveals several interesting features [30]. The *Z* configuration of the aroylhydrazone with respect to N2–C9 bond is retained in all complexes. The C7–N1 bond length of the metal free ligand, 1.277(2) \AA , increases to 1.305(3), 1.299(3) and 1.298(5) \AA in complexes **1–3**, respectively. The slight increase in N1–N2 bond distances 1.393(3), 1.401(3) and 1.403(4) \AA , respectively, in complexes **1–3** from 1.369(2) \AA confirms increase in electron delocalization on complexation. Since the aroylhydrazone is coordinated in the iminolate form, the C9–O2 bond is expected to assume a single bond character, but due to electron delocalization in the coordinated ligand, the actual bond distances lie between the distances expected for C–O and C=O [43, 44]. The C9–O2 bond lengths are 1.326(3), 1.327(3) and 1.313(5) \AA , respectively, in complexes **1–3**. In addition to this, the C9–N2 bond distances 1.292(3), 1.296(3) and 1.302(5) \AA are closer to C=N distances due to enolization on complexation. The oxido oxygen (O4/O5) and N atom, N3, of heterocyclic base occupy the axial positions of the distorted octahedron. The central metal atom, molybdenum, is displaced toward the axial oxido oxygen (O4/O5) from the mean square plane defined by equatorial donor atoms (O1, N1, O2, O4/O5) by 0.3255, 0.3298 and 0.3348 \AA for complexes **1–3**, respectively.

The aroylhydrazone ligand is coordinated in the meridional fashion forming five- and six-membered chelate rings with intraligand bite angles O(1)–Mo(1)–N(1), 80.30(7) $^\circ$, 80.14(7) $^\circ$ and 80.01(11) $^\circ$, respectively, for complexes **1–3** and O(2)–Mo(1)–N(1), 72.83(7) $^\circ$, 72.23(7) $^\circ$ and 72.84(11) $^\circ$,

Fig. 1 ORTEP plot of the molecular structure of $[\text{MoO}_2(\text{CAB})(\text{py})]$ (**1**) with displacement ellipsoids at 30% probability level along with atom numbering scheme of the non-hydrogen atoms. (Color figure online)

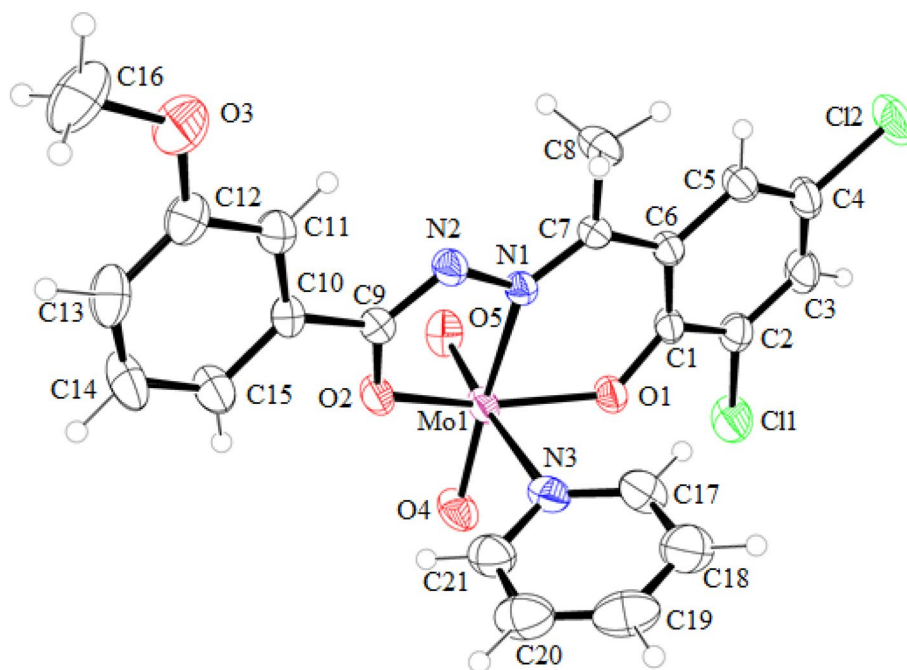
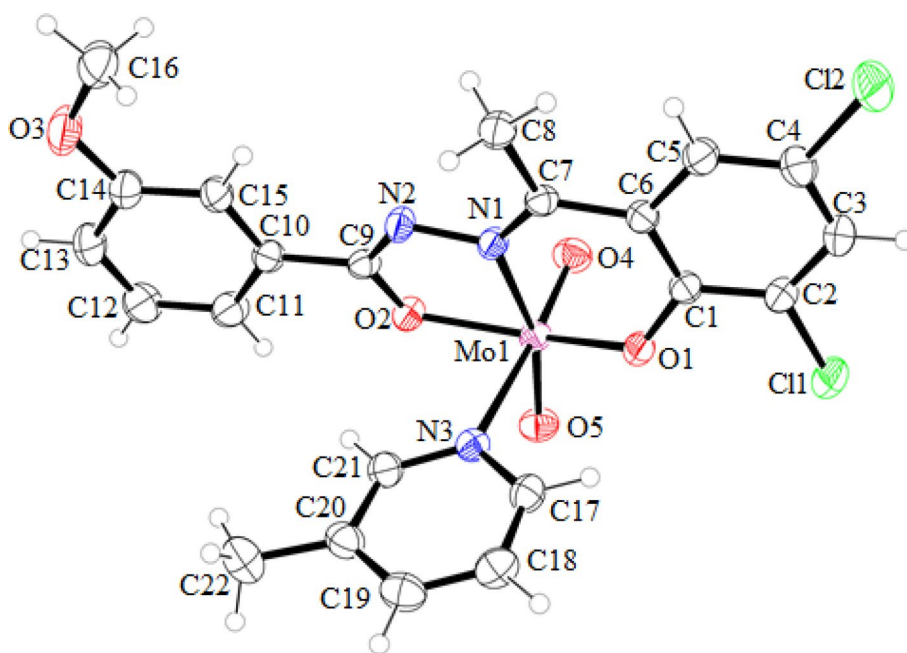


Fig. 2 ORTEP plot of the molecular structure of $[\text{MoO}_2(\text{CAB})(3\text{-pic})]$ (**2**) with displacement ellipsoids at 30% probability level along with atom labeling scheme of the non-hydrogen atoms. (Color figure online)



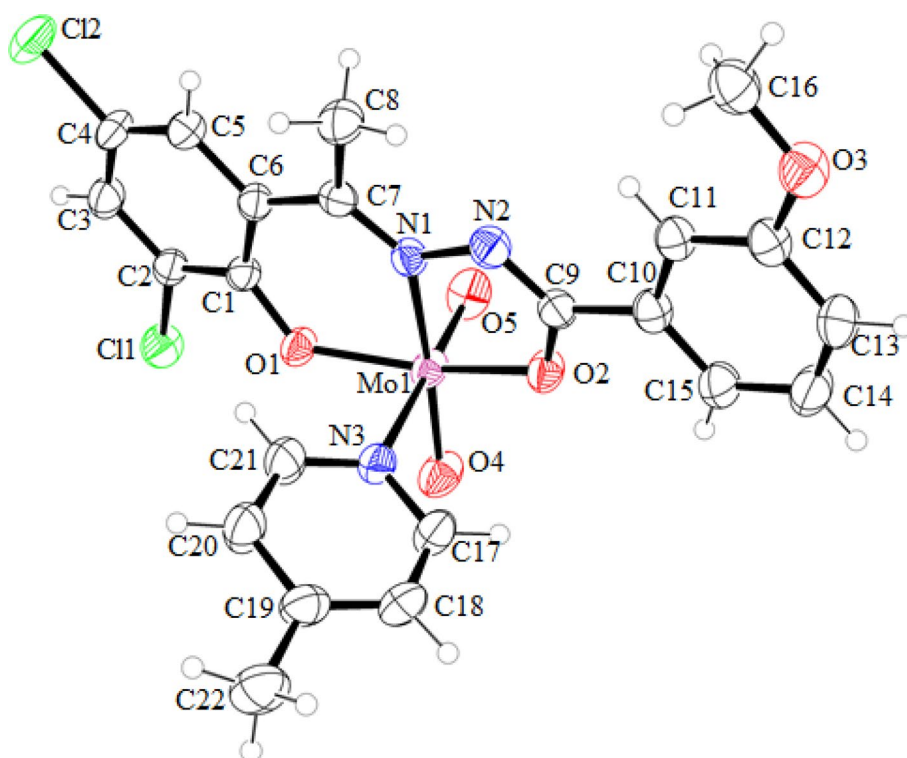
respectively, for complexes **1–3** [40, 41]. The dihedral angle between five and six membered metallocycles fused along Mo(1)–N(1) junction is found to be $9.83(4)^\circ$, $9.52(5)^\circ$ and $7.167(8)^\circ$ for complexes **1–3**, respectively. As a result of *trans* influence of oxido oxygen, Mo(1)–N(3) bond distances are considerably larger than Mo–N1 bond distances.

Similar to other reported complexes, oxido oxygens (O4 and O5) are mutually *cis* and Mo(1)=O(4) and Mo(1)=O(5) bond distances fall in the range 1.68–1.71 Å. This is also confirmed from O(4)–Mo(1)–O(5) bond angles [40, 41]. The

tetragonality or tetragonal distortion parameter, T values of 0.9505, 0.9442 and 0.9449 Å, in complexes **1–3**, respectively, indicates slight distortion from regular octahedral coordination geometry in these complexes. The bond distances to molybdenum are in the order Mo–O_(oxido) < Mo–O_(phenolic) < Mo–O_(iminolate) < Mo–N_(azo) < Mo–O_(solvent).

In all the complexes, the gathering of molecules in the particular manner in the unit cell results in hydrogen bonding and π – π interactions. In complex **1**, three intermolecular non-conventional hydrogen bonding interactions in which the

Fig. 3 ORTEP plot of the molecular structure of $[\text{MoO}_2(\text{CAB})(4\text{-pic})]$ (**3**) with displacement ellipsoids at 30% probability level along with atom labeling scheme of the non-hydrogen atoms. (Color figure online)



oxido oxygens, O4 and O5, behave as acceptor generates a two-dimensional supramolecular architecture (Table S4 and Figs. 4 and 5). The bifurcated hydrogen bond between O5 and hydrogens H5 and H8A gives rise to a $R_2(6)$ motif (Fig. 5). The hydrogen bonding interactions present in the system give a two-dimensional supramolecular architecture (Table S4 and Fig. 6) in complex **2**, and the $\text{C3-H3}\cdots\text{Cl2}$ hydrogen bonding interaction resulted in a $R_2^2(8)$ motif (Fig. 7). In complex **3**, similar to other complexes due to the presence of several oxygens and chlorine atoms, four non-conventional intermolecular hydrogen bonding interactions are present in the system. The different hydrogen bonding interactions present in the system gave a three-dimensional supramolecular architecture to the complex (Table S4 and Fig. 7). In complex **1**, the centroids Cg(1) and Cg(4) involved in π - π interaction with Cg(3) and Cg(5), respectively, at a distance of 3.841(18) and 3.844(18) Å contribute to the stability of packing (Table S4 and Fig. 8). The π - π interactions observed in the crystal system resulted in a one-dimensional supramolecular architecture. In complexes **2** and **3**, the supramolecular arrangement is strengthened by $\text{Cg}(1)\cdots\text{Cg}(3)$ and $\text{Cg}(4)\cdots\text{Cg}(5)$ interactions (Table S4 and Fig. 9).

Hirshfeld surface analysis and the 2D fingerprint plot

The HSs mapped over d_{norm} , shape index and curvedness are shown in Fig. 10. The predominant interatomic

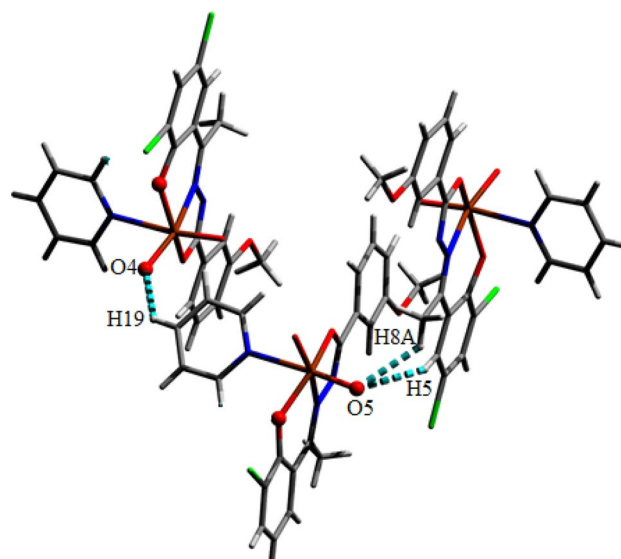


Fig. 4 Hydrogen bonding interactions of complex **1**. (Color figure online)

contacts are represented as red spots on the d_{norm} surface. In the HSs mapped with a shape index plot, the presence of red and blue triangles (bow-tie pattern) highlighted by red dotted circle in all complexes clearly indicates the presence of π - π stacking interactions. The appearance of flat surfaces delineated by a blue outline in HS mapped over curvedness is another evidence for π - π stacking

Fig. 5 2D supramolecular network formed by hydrogen bonding interactions and the ring motif formed is highlighted in yellow for complex **1**. (Color figure online)

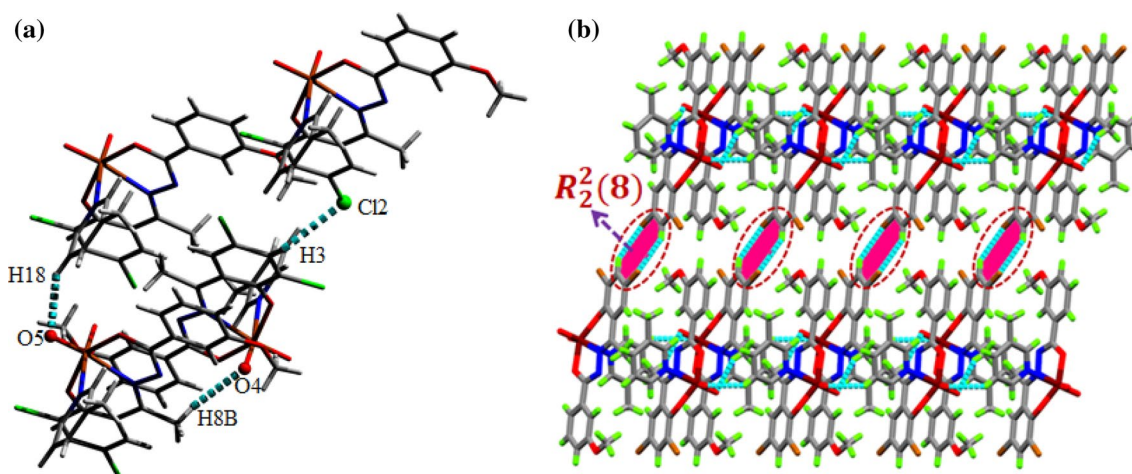
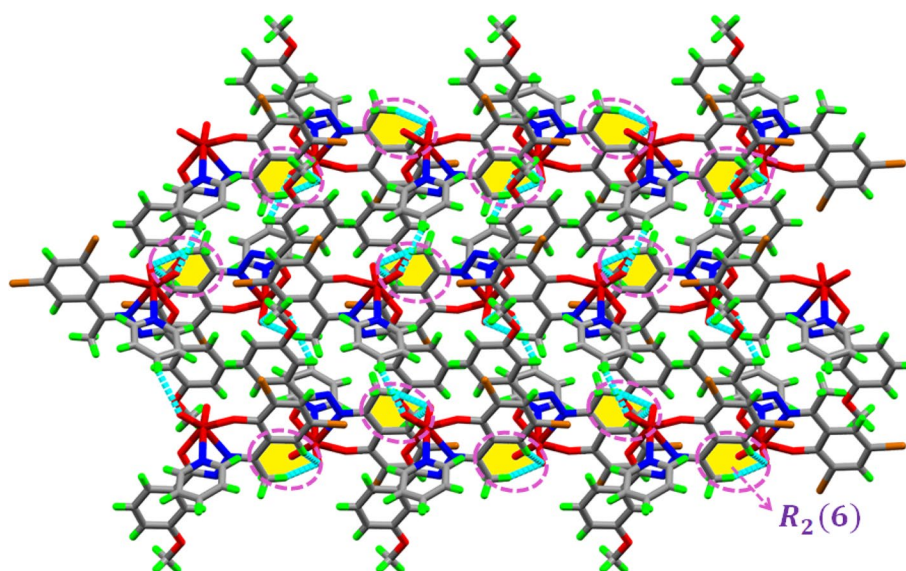


Fig. 6 **a** Hydrogen bonding interactions of complex **2**. **b** 2D supramolecular network formed by hydrogen bonding interactions and the ring motif formed is highlighted in red circles for complex **2**. (Color figure online)

interactions (Fig. 10). The bow-tie pattern for complexes in the HSs mapped with shape index function is displayed in Fig. S6.

The percentage contributions of various intermolecular contacts represented by two-dimensional fingerprint plots with d_i and d_c ranging from 1.0 to 2.8 Å are presented in Fig. 11. The H...H contacts occupy a major share of the HS for all the complexes. The O...H/H...O interactions cover the next largest region of the fingerprint plot and appeared as 21.3, 23.2 and 23.9%, respectively, for complexes **1–3**. Due to the presence of coordinated pyridine and picoline molecule, the C...H/H...C interaction which is concentrated highly at the edges contributes significantly to the HS. The N...H/H...N interactions contribute negligibly to the total Hirshfeld surface. The C...C contacts mirrored at the diagonals represent π - π stacking interactions and occupy 5.7, 4.6

and 6.1%, respectively, for complexes **1 to 3**. The absence of halide-halide interaction is also evident from Hirshfeld surface. The fingerprint plot analysis shows that weak interactions contribute significantly to the packing of molecules. The relative contributions of various significant interactions are represented as a histogram, and the contribution of low percentage interactions is represented as others (Fig. S7). The histogram reveals that low percentage interactions also contribute to the packing of molecule.

Interaction energy calculations and energy framework analysis

The interaction energy calculations for complexes **1–3** presented in Table 2 reveal that the highest total interaction energy (-116.6 , -118.3 and -119.6 kJ mol $^{-1}$ for

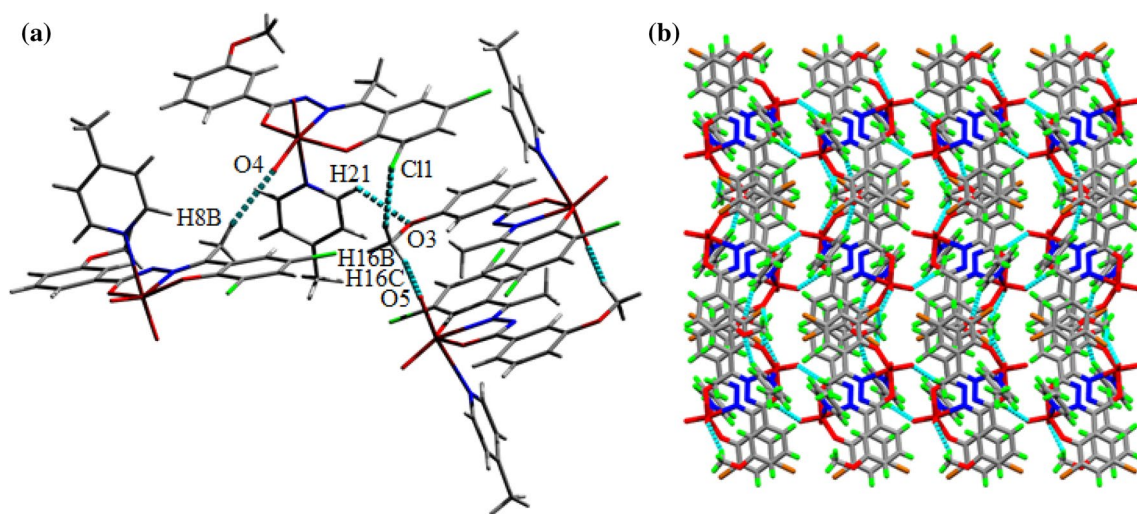
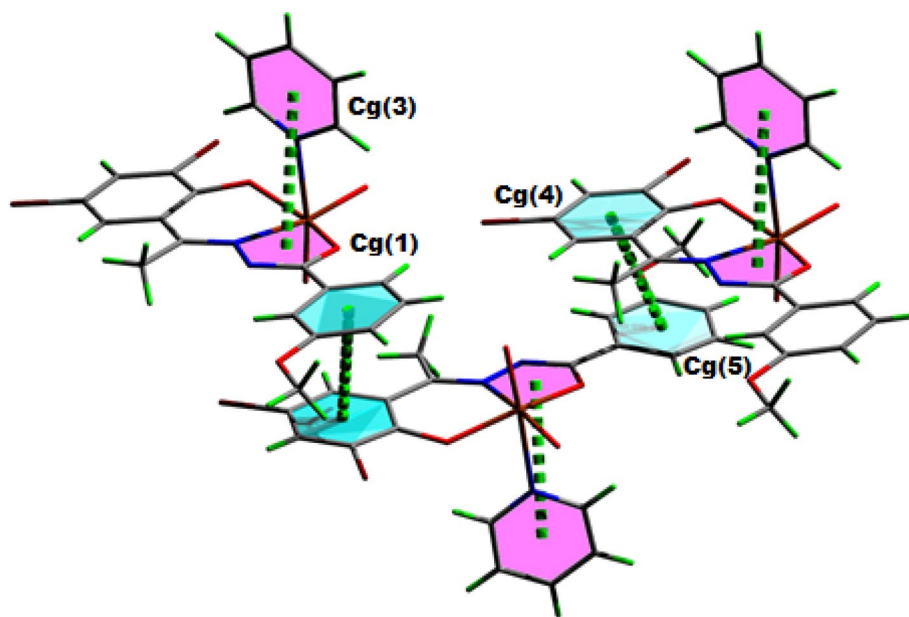


Fig. 7 a H-bonding interactions and b 3D supramolecular network formed by hydrogen bonding interactions of complex **3**. (Color figure online)

Fig. 8 1D supramolecular chain formed by π - π interactions for complex **1**. (Color figure online)



complexes **1**, **2** and **3**, respectively) is shown by the green (for complex **1** and **3**) or red (for complex **2**) colored molecule with symmetry operation, $(-x, -y, -z)$ located at distances of 5.77, 5.61 and 5.99 Å from the centroid of the selected molecule for complexes **1**, **2** and **3**, respectively (Table S5 and Fig S4). For the complex **1**, the orange colored molecule with same symmetry operation located at a distance of 10.97 Å from the centroid of the selected molecule shows the lowest total interaction energy (-3.4 kJ mol^{-1}). In complex **2**, the blue colored molecule $(x + 1/2, -y + 1/2, z + 1/2)$ at 13.46 Å has the lowest interaction energy (-2.5 kJ mol^{-1}). For complex **3**, the violet colored molecule with lowest interaction energy

(-1.4 kJ mol^{-1}) is located at a distance of 12.32 Å (symmetry operation $-x, y + 1/2, -z + 1/2$).

The average interaction energy values for complexes **1**, **2** and **3** are found to be -293.6 , -321.6 and -305 kJ mol^{-1} , respectively (Table 2). The interaction energy is dominated by dispersion energy framework for all complexes (-298.2 , -359.9 and $-328.4 \text{ kJ mol}^{-1}$, respectively) [40]. The result also establishes that the complex **2** is found to be energetically more stable. The stability follows the order complex **2** > complex **3** > complex **1**.

The energy framework analysis gives a three-dimensional topological representation of the interaction in which the radius of the cylinder is proportional to the magnitude of the interaction energy (Fig S8). The

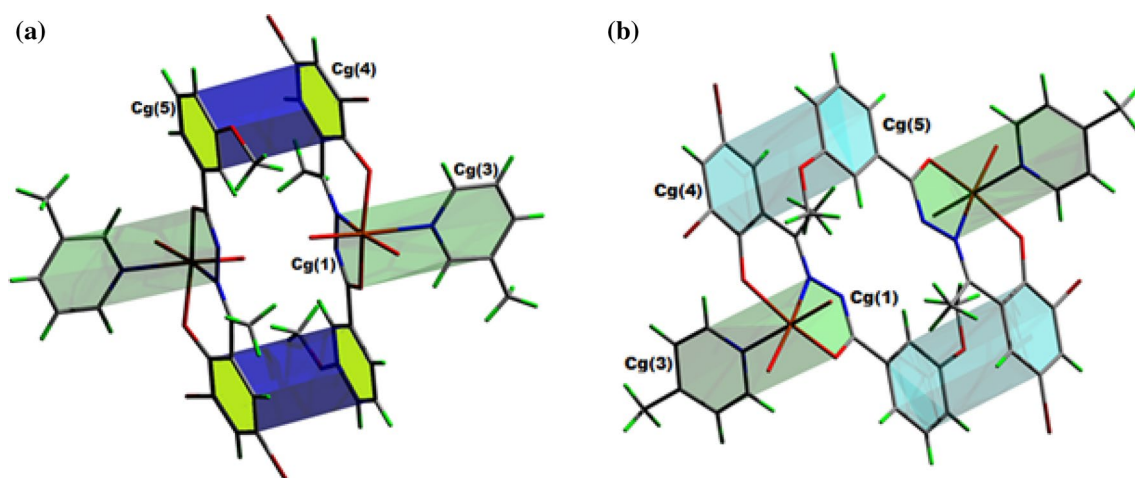
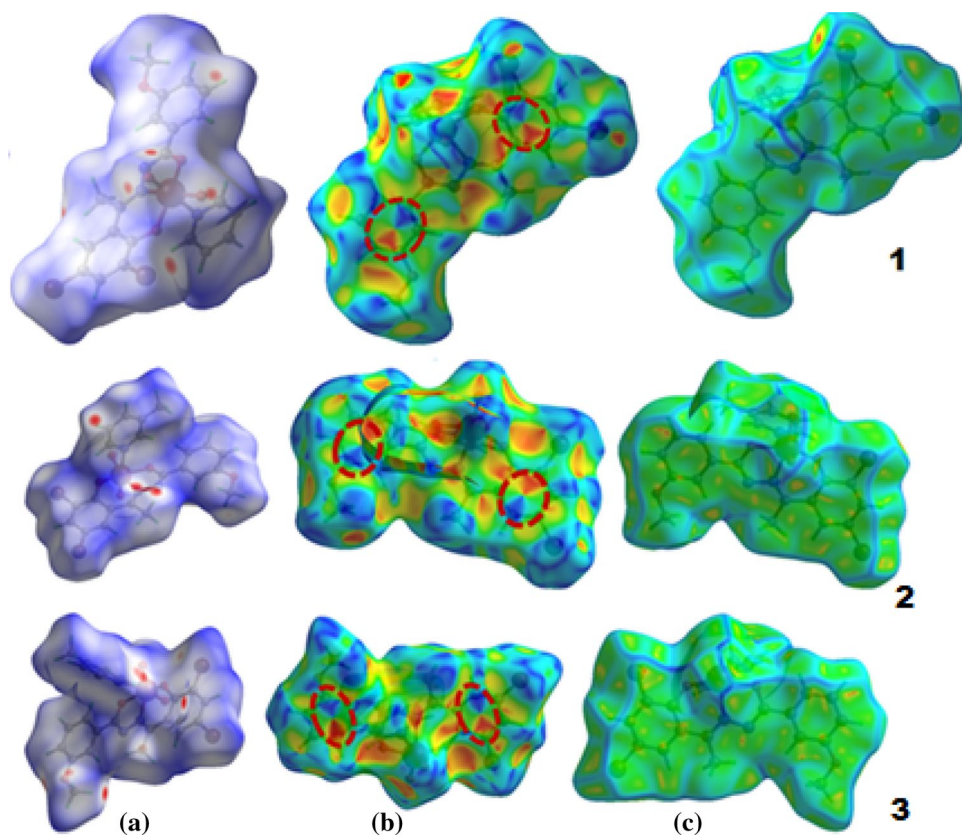


Fig. 9 $\pi\cdots\pi$ interactions of complexes **2** and **3**. (Color figure online)

Fig. 10 Hirshfeld surfaces mapped over **a** d_{norm} , **b** shape index and **c** curvedness for **1–3**. (Color figure online)



thickness of the cylinder represents the relative strength of molecular packing in different directions. The cylinders corresponding to π - π stacking interactions are shown as thick tubes or pillars in these crystal structures.

Free radical scavenging studies

The radical scavenging activity of aroylhydrazone, H₂CAB and the molybdenum(VI) complexes are investigated using

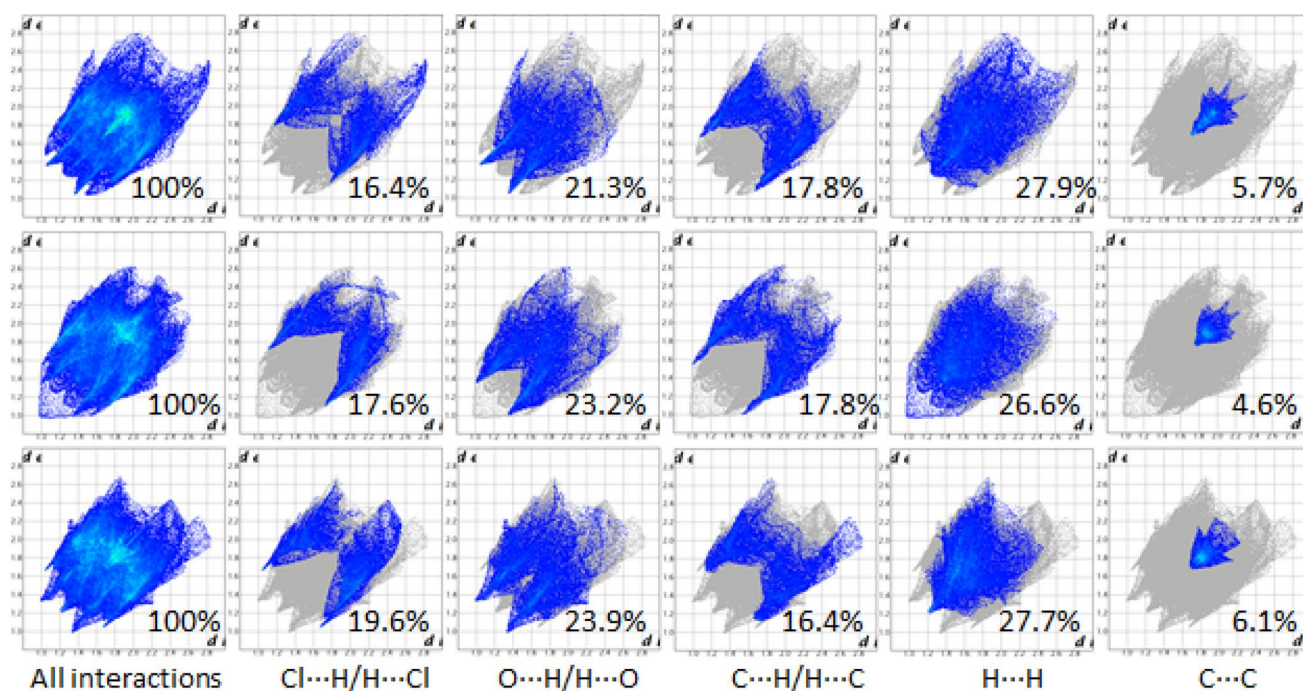


Fig. 11 2D finger print plots for complexes **1**, **2** and **3** with d_e and d_i ranging from 1 to 2.8 Å and their plots delineated into different major contact types. (Color figure online)

Table 2 Interaction energies calculated from the CrystalExplorer (kJ/mol)

	E'_{ele}	E'_{pol}	E'_{dis}	E'_{rep}	E_{tot}	Average E_{tot}
Complex 1	− 98.7	− 39.4	− 298.2	142.7	− 279.17	− 293.6
Complex 2	− 94.4	− 43.2	− 359.9	175.9	− 305.93	− 321.6
Complex 3	− 98	− 45	− 328.4	166.4	− 290.1	− 305

DPPH assay. The absorbance of DPPH[•] is found to be decreased significantly in the presence of aroylhydrazone and does show a remarkable change in the case of complexes (Fig. S9). This shows that ligands show good free radical scavenging activity compared to corresponding complexes. The decrease in absorbance in the presence of aroylhydrazone may be due to the formation of stable DPPH-H compound (Fig. 12). The IC₅₀ value of H₂CAB-H₂O was found to be 58.39 μg/mL. This can be explained by hydrogen atom transfer (HAT) mechanism. Aroylhydrazone contains two abstractable hydrogens (phenolic and imine hydrogen), and no such hydrogens are present in complexes **1**, **2** and **3**. Hydrogen abstraction depends on bond dissociation energy. The lower the bond dissociation energy, the more favorable will be the site for H-abstraction. The bond dissociation energy was approximately 390 and 460 kJ/mol for N–H and O–H, respectively. Based on this, we can conclude that imine hydrogen was abstracted. In addition to this as evident from single-crystal X-ray diffraction studies, the hydrogen atom abstraction from phenolic ring is quite difficult under examined conditions due to the formation of strong intramolecular

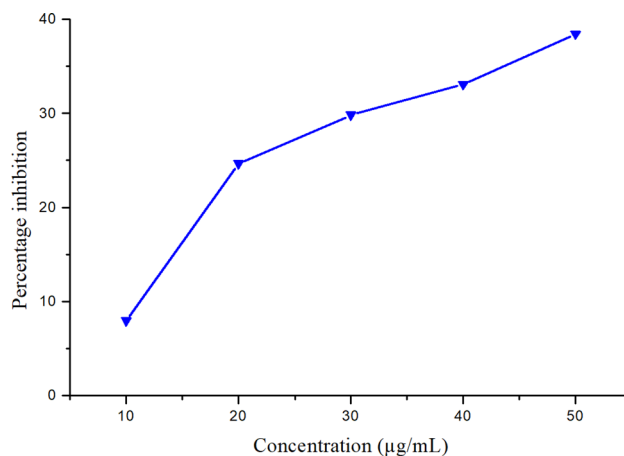
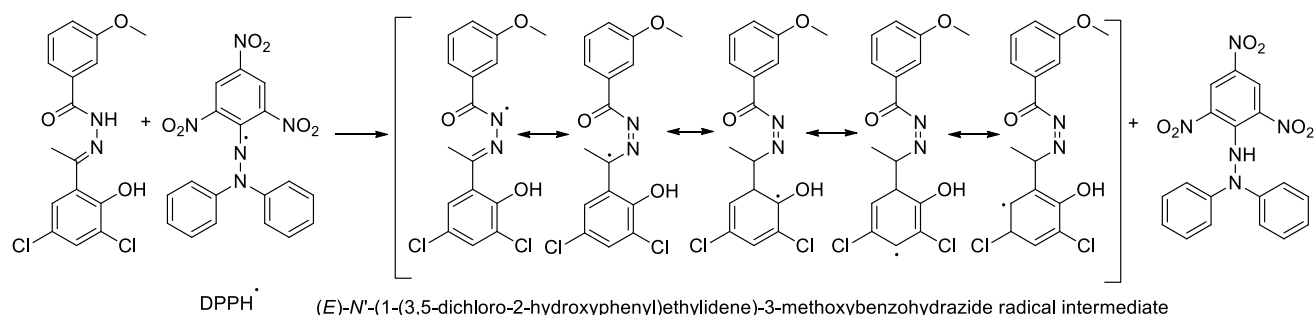


Fig. 12 Plot of percentage inhibition versus drug concentration for aroylhydrazone H₂CAB. (Color figure online)

hydrogen bond with azomethine nitrogen [30]. The reaction of DPPH radical may generate nitrogen (N[•])-centered radical (hydrazoneyl radical which is stabilized through conjugation



Scheme 2 Plausible reaction of DPPH with H_2CAB

(Scheme 2)) [45, 46]. Due to the absence of such hydrogens, the complexes presented in this study do not show free radical scavenging activity.

Conclusion

The present paper deals with the synthesis of a three *cis*- MoO_2 complexes derived from an ONO donor aroylhydrazone with the sixth coordination site occupied by different heterocyclic bases. The complexes were characterized using various physicochemical techniques. All three complexes are structurally characterized by single-crystal X-ray diffraction studies. The aroylhydrazone behaves as a dianionic tridentate ligand and coordinates to the metal center in the tautomeric iminolic form. The complexes exhibit distorted octahedral geometry. The pivotal role of hydrogen bonding and weak non-covalent forces in the development of supramolecular framework are investigated. Hirshfeld surface analysis reproduces the upshots of crystal structure studies, and the role of hydrogen bonding interactions in the development of diverse supramolecular architecture is also well established. The various intermolecular contacts including low percentage interactions were identified and quantified using associated 2D fingerprint plot. The interaction energy calculation reveals that the dispersion energy component dominates over electrostatic, polarization and repulsion energy component. Complex **2** is energetically more stable than complexes **1** and **3**. Due to the presence of abstractable hydrogen, aroylhydrazones show free radical scavenging activities, whereas the complexes are inactive.

Supporting information

The tables and figures including hydrogen bonding and non-bonding interactions, IR, UV–Vis and Hirshfeld surface analysis are included.

Supplementary data

Crystallographic data for the structural analysis have been deposited with the Cambridge Crystallographic Data Center as CCDC 1972050, 1972051 and 1972058 for complexes $[\text{MoO}_2(\text{CAB})(\text{py})]$ (**1**), $[\text{MoO}_2(\text{CAB})(3\text{-pic})]$ (**2**) and $[\text{MoO}_2(\text{CAB})(4\text{-pic})]$ (**3**), respectively. Copies of this information may be obtained free of charge via www.ccdc.cam.ac.uk/conts/retrieving.html or from the Director, CCDC, 12 Union Road, Cambridge, CB2, 1EZ, UK (fax: +44-1223-336-033; e-mail: deposit@ccdc.cam.ac.uk).

Acknowledgements DK thanks the University Grants Commission, New Delhi, India, for the award of a Senior Research Fellowship (F.17-45/2008(SA-1) dated 11.08.2014). The authors are thankful to the Sophisticated Analytical Instrumentation Facility, Cochin University of Science and Technology, Kochi, India, for elemental analyses, $^1\text{H-NMR}$ spectra and single-crystal X-ray diffraction measurements.

Compliance with ethical standards

Conflict of interest The authors declare that they have no conflict of interest.

References

- Peng H, Peng X, Huang J, Huang A, Xu S, Zhou J, Huang S, Cai X (2020) *J Mol Struct* 4:5. <https://doi.org/10.1016/j.molstruc.2020.128138>
- Bakir M, Conry R (2016) *J Coord Chem* 69:1244–1257
- Kuriakose D, Aravindakshan AA, Kurup MRP (2017) *Polyhedron* 127:84–96
- Asha TM, Kurup MRP (2020a) *Transit Met Chem* 45:467–476
- Nair RS, Kuriakose M, Somasudaram V, Shenoi V, Kurup MRP, Srinivas P (2014) *Life Sci* 116:90–97
- Bakale RP, Naik GN, Mangannavar CV, Muchchandi IS, Shcherbakov IN, Frampton C, Gudasi KB (2014) *Eur J Med Chem* 73:38–45
- Ebrahimipour SY, Sheikhshoae I, Simpson J, Ebrahimnejad H, Dusek M, Kharazmi N, Eigner V (2016) *New J Chem* 40:2401–2412
- Rocha CS, Filho LFOB, de Souza AE, Diniz R, Denadai ÂML, Beraldo H, Teixeira LR (2019) *Polyhedron* 170:723–730

9. He L-Y, Qiu XY, Cheng JY, Liu SJ, Wu SM (2018) *Polyhedron* 156:105–110
10. Saif M, El-Shafiy HF, Mashaly MM, Eid MF, Nabeel AI, Fouad R (2016) *J Mol Struct* 1118:75–82
11. Dinda R, Panda A, Banerjee A, Mohanty M, Pasayat S, Tiekink ERT (2020) *Polyhedron*. <https://doi.org/10.1016/j.poly.2020.114533>
12. Asha TM, Kurup MRP (2018) *Inorg Chim Acta* 483:44–52
13. Asha TM, Kurup MRP (2019) *Polyhedron* 169:151–161
14. Mondal J, Manna AK, Patra GK (2018) *Inorg Chim Acta* 474:22–29
15. Guerrero T, Lacroix PG, García-Ortega H, Morales-Saavedra OG, Agustin D, Farfán N (2016) *Inorg Chim Acta* 442:10–15
16. Zhang WQ, Atkin AJ, Fairlamb IJ, Whitwood AC, Lynam JM (2011) *Organometallics* 30:4643–4654
17. Anaconda JR, Rincones M (2015) *Spectrochim Acta A* 141:169–175
18. Fousiamol MM, Sithambaresan M, Smolenski VA, Jasinski JP, Kurup MRP (2018) *Polyhedron* 141:60–68
19. Mangalam NA, Sivakumar S, Kurup MRP, Suresh E (2010) *Spectrochim Acta A* 75:686–692
20. Biswal D, Pramanik NR, Chakrabarti S, Drew MGB (2016) *Inorg Chim Acta* 451:92–101
21. Wu CD, Ngo HL, Lin W (2004) *Chem Commun* 14:1588–1589.
22. Evans OR, Ngo HL, Lin W (2001) *J Am Chem Soc* 123:10395–10396
23. Cho SH, Ma B, Nguyen ST, Hupp JT, Albrecht-Schmitt TE (2006) *Chem Commun* 2563–2565
24. Maurya MR, Dhaka S, Avecilla F (2014) *Polyhedron* 67:145–159
25. Bagherzadeh M, Zare M (2013) *J Coord Chem* 66:2885–2900
26. Ebrahimipour SY, Khabazadeh H, Castro J, Sheikhshoaei I, Crochet A, Fromm KM (2015) *Inorg Chim Acta* 427:52–61
27. Kuriakose D, Kurup MRP (2020) *J Mol Struct*. <https://doi.org/10.1016/j.molstruc.2020.128188>
28. SMART and SAINT (1997) Area detector software package and SAX area detector integration program. Bruker Analytical X-ray, Madison
29. SADABS (1997) Area detector absorption correction program. Bruker Analytical X-ray, Madison
30. Sheldrick GM (2015) *Acta Cryst C* 71:3–8
31. Farrugia LJ (2012) *J Appl Cryst* 45:849–854
32. Brandenburg K (2011) Diamond version 3.2g, Crystal Impact GbRBonn, Germany
33. MERCURY 3.10.1 Supplied with Cambridge Structural Database 2016 CCDC, Cambridge
34. Turner MJ, McKinnon JJ, Wolff SK, Grimwood DJ, Spackman PR, Jayatilaka D, Spackman MA (2017) *CrystalExplorer17*, University of Western Australia
35. Spackman MA, McKinnon JJ (2002) *CrystEngComm* 4:378–392
36. McKinnon JJ, Jayatilaka D, Spackman MA (2007) *Chem Commun* 3814–3816
37. Spackman MA, Jayatilaka D (2009) *CrystEngComm* 11:19–32
38. Mackenzie CF, Spackman PR, Jayatilaka D, Spackman MA (2017) *IUCrJ* 4:575–587
39. Turner MJ, Grabowsky S, Jayatilaka D, Spackman MA (2014) *J Phys Chem Lett* 5:4249–4255
40. Kuriakose D, Kurup MRP (2019) *Polyhedron* 170:749–761
41. Kuriakose D, Kurup MRP (2020) *J Mol Struct*. <https://doi.org/10.1016/j.molstruc.2019.127467>
42. Mangalam NA, Kurup MRP (2011) *Spectrochim Acta A* 78:926–934
43. Raj BNB, Kurup MRP, Suresh E (2008) *Spectrochim Acta A* 71:1253–1260
44. Mangalam NA, Sheeja SR, Kurup MRP (2010) *Polyhedron* 29:3318–3323
45. Harej M, Dolenc D (2007) *J Org Chem* 72:7214–7221
46. Belkheiri N, Bouguerne B, Bedos-Belval F, Duran H, Bernis C, Salvayre R, Nègre-Salvayre A, Baltas M (2010) *Eur J Med Chem* 45:3019–3026

Publisher's Note Springer Nature remains neutral with regard to jurisdictional claims in published maps and institutional affiliations.